Energy 285 (2023) 129505

Contents lists available at ScienceDirect

Energy

journal homepage: www.elsevier.com/locate/energy

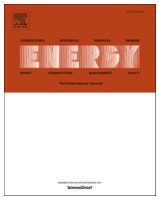

Optimized lower pressure limit for condensate underground gas storage using a dynamic pseudo-component model

Peng Deng [a,b], Zhangxin Chen [b,c,d,*], Xiaolong Peng [a], Jianfeng Wang [e], Suyang Zhu [a], Haoming Ma [b], Zhengbin Wu [f]

[a] State Key Laboratory of Oil and Gas Reservoir Geology and Exploitation, Southwest Petroleum University, Chengdu, PR China
[b] Department of Chemical and Petroleum Engineering, University of Calgary, 2500 University Drive NW, Calgary, Alberta, Canada
[c] College of Petroleum Engineering, China University of Petroleum, Beijing, PR China
[d] Eastern Institute for Advanced Study, Ningbo, PR China
[e] Northwest Oilfield Company, China Petro-Chemical Corporation, Urumqi, PR China
[f] School of Resources, China University of Geosciences (Wuhan), Wuhan, PR China

ARTICLE INFO

Handling editor: A. Olabi

Keywords:
Condensate underground gas storage
Natural gas injection
Pseudo-component simulation
Lower pressure limit

ABSTRACT

In the context of gas injection in reservoirs, the dilution process of components' thermodynamic properties has not been adequately represented in traditional numerical simulation methods. This study focuses on the Dalaoba condensate underground gas storage (CUGS) in China and establishes a dynamic pseudo-component model to identify the equilibrium point for gas storage facility efficiency and the condensate oil recovery rate. Using a multi-objective particle swarm optimization approach, thermodynamic parameters are estimated as functions of the injected gas volume. This dynamic pseudo-component model is then utilized to find the optimized lower pressure limit for CUGS by assessing condensate oil production, gas flow capability, and water encroachment. Results show that the dynamic pseudo-component model can represent the process of thermodynamic property changes towards lighter components during natural gas injection. The case study demonstrates that conventional models overestimate condensate oil production, while the dynamic model achieves an accuracy rate of 92.8 % with historical data. The dynamic pseudo-component model offers valuable insights for large-scale gas injection simulation, promoting stable and efficient natural gas storage and supply in CUGS.

1. Introduction

As clean and efficient natural gas gradually gains importance in the new energy landscape, underground gas storage (UGS) facilities have become increasingly recognized for their peak-shaving capability. These facilities, characterized by summer injection and rapid winter production, play a crucial role in today's energy market by meeting expanding consumer demand. A recent report by the International Energy Agency (IEA) indicates that UGS capacity has now reached 110 billion cubic meters in the United States and 98 billion cubic meters in the European Union [1]. UGS facilities can be developed using various media, including depleted reservoirs, salt caverns, and aquifers, as shown in Fig. 1. Salt caverns and aquifers are common geological formations worldwide. However, assessing their suitability for gas storage requires thorough evaluations considering factors like sealing, connectivity, and volume [2–4]. While salt caverns have been extensively studied in Europe, depleted reservoirs remain the preferred choice because of their enhanced safety, ample storage capacity, and cost-effectiveness all over the world. For depleted reservoirs among the three underground storage types, as depicted in Fig. 2, China, the United States, Canada, and the European Union have adoption rates of 93 %, 87 %, 78 %, and 58 %, respectively [1,5–7].

In case where depleted gas reservoirs are repurposed as UGS facilities, the practice of repurposing depleted condensate gas reservoirs is becoming increasingly popular [8–10]. One primary reason for this trend is that depleted condensate gas reservoirs often contain a significant amount of condensate oil in a layer that has not been fully recovered [11]. This situation has caused numerous oil and gas projects to operate at a loss, posing a significant challenge for the industry [12]. In some high condensate oil content reservoirs, the condensate oil recovery factor can be as low as 30 %, meaning that around 70 % of crude oil remains unrecovered in the reservoir [13–15]. Rebuilding a depleted

* Corresponding author. Department of Chemical and Petroleum Engineering, University of Calgary, 2500 University Drive NW, Calgary, Alberta, Canada.
E-mail address: zhachen@ucalgary.ca (Z. Chen).

https://doi.org/10.1016/j.energy.2023.129505
Received 8 May 2023; Received in revised form 26 September 2023; Accepted 27 October 2023
Available online 28 October 2023

condensate gas reservoir as condensate underground gas storage (CUGS) involves injecting substantial amounts of natural gas during an off-peak natural gas demand season. This process can help restore formation pressure and facilitate the retrograde vaporization of condensate oil into a gas phase. As a result, this helps to restore a reservoir's mobility and gradually produces the original, heavier condensate components during a subsequent natural gas peak season [16]. Therefore, transforming a nearly exhausted condensate gas reservoir into CUGS not only helps achieve stable energy supply targets but also improves the condensate oil recovery factor and reduces the amount of wasted condensate oil resources [8].

However, CUGS facilities operation is different from the conventional development of condensate gas reservoirs. In traditional development, it has become widely accepted that maintaining the reservoir pressure close to or above the dew point pressure through cyclic gas injection helps to minimize condensate oil accumulation [17,18]. On the other hand, when a condensate gas reservoir is converted into a CUGS facility, it must meet a large-scale gas production requirement [19–21]. As shown in Fig. 3, if the pressure is maintained above or near the dew point during this operation, the CUGS can minimize condensate precipitation and water encroachment but will face a limited working gas capacity, which will compromise its ability to provide substantial amounts of natural gas in peak demand season. Furthermore, excessively high pressure can lead to fracture activation and increased risk of gas leakage [22–24]. In contrast, operating below the dew point results in a larger working gas capacity, however, it also leads to considerable condensate oil precipitation and water encroachment for CUGS. These issues represent the primary technical obstacles and economic risks faced by such facilities [25,26]. Therefore, a relatively safe development method for CUGS facilities is to find the optimal lower pressure limit, which keeps reservoir contamination within a controllable range, and gradually remove condensate oil through multiple injection and production cycles [27–29]. Naturally, this requires a thorough understanding of the actual conditions and phase transitions within the CUGS.

Due to the high computing requirements and long calculation time of fully compositional simulation, a pseudo-component technique is frequently utilized in a CUGS simulation model [18,30,31]. The general approach is to adjust the molar fractions of pseudo-components at each time step while keeping other component thermodynamic properties constant to simulate phase transition processes [32,33]. This traditional numerical simulation method is accurate in simulating the depletion development stage of a condensate gas reservoir, but it fails to calculate the phase change process for a CUGS precisely as an amount of injected natural gas almost entirely replaces the original condensate gas during injection process [18,34]. Heavy component condensate fluids underground mix with the newly injected light component natural gas, causing dramatic changes in the thermodynamic properties of the original pseudo-components [30,35,36]. As a result, the key fluid properties, such as the dew point, bubble point, viscosity, and other parameters calculated using the original pseudo-component thermodynamic properties are no longer accurate.

In this research, we established a dynamic pseudo-component model that links the relationship between the thermodynamic properties of pseudo-components and the amount of injected natural gas. Using the Dalaoba CUGS as an example, we simulated the lower pressure limit of this facility. When compared to the traditional pseudo-component model, the dynamic model increases the workload of fluid property experiments. However, it facilitates the accurate determination of thermodynamic properties under varied natural gas injection levels, thereby enhancing the precision of fluid properties and flow states in CUGS simulations. The rest of this paper is structured as follows: Section 2 describes the key geological and phase information for the Dalaoba CUGS in China. Section 3 analyzes the dynamic pseudo-component simulation model from governing equations and fluid flow. Section 4 applies the dynamic approach to history matching for 25 years and predicts the lower pressure limit for the upcoming five years. Section 5 summarizes the key findings of this work.

2. Study area

UGS construction in China began in the late 1960s and has entered a period of rapid growth over the past five years. The number of UGS facilities in China has reached 22, with more than 500×10^8 m^3 storage capacity and 180×10^8 m^3 working capacity. Most of the UGS facilities in China are built in depleted oil and gas fields, and only two of them are situated in salt caverns [21].

The Dalaoba reservoir is situated in the northern part of the Tarim Basin, covering an area of nearly 7.6 km^2, as shown in Fig. 4. The formation is approximately 25–35 m thick and is primarily distributed across two sub-layers [37,38]. The upper layer has experienced relatively high recovery of condensate gas in recent years, is where the Dalaoba CUGS facility located. The middle interlayer is a mudstone layer with a thickness of about 140–160 m. Given this significant mudstone barrier, the issue of evaporation from the lower layer is not taken into consideration.

The Dalaoba CUGS facility is situated in a depleted condensate gas reservoir, renowned for its high pressure and considerable content of condensate oil. The reservoir lies at a depth of approximately 5000 m,

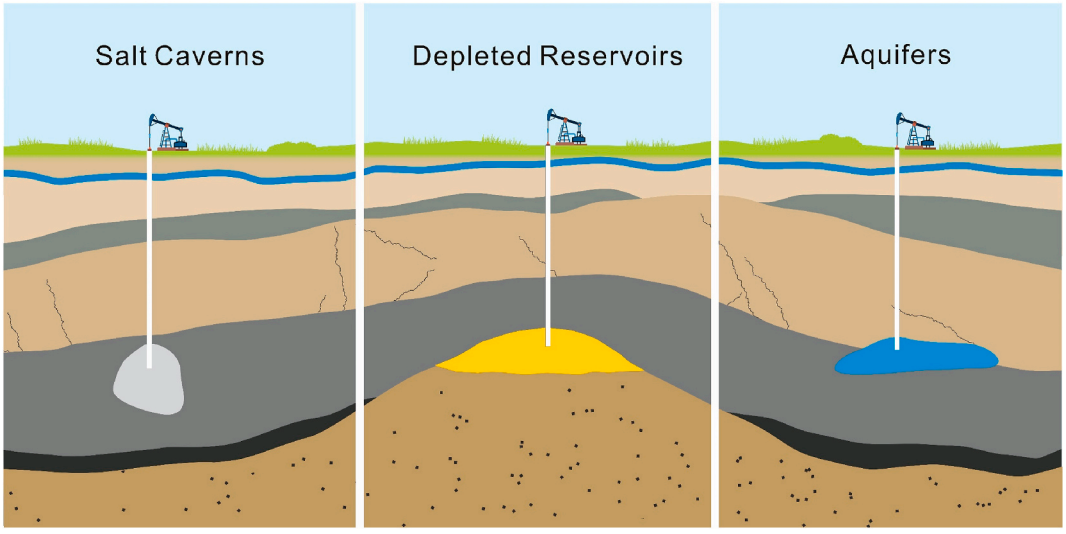

Fig. 1. Three main types of UGS.

which generates an initial pressure of over 50 MPa [39]. Additionally, the reservoir contains a substantial amount of condensate, with a content of around 750 g/m^3, which significantly complicates the process of condensate oil recovery. As a result, at the conclusion of the depletion development stage roughly 64 % of condensate oil remains, presenting significant challenges to the construction of this storage facility.

Since there is still a large amount of condensate oil remaining in the reservoir, it is crucial to design a reasonable lower pressure limit. If the lower pressure limit is too low, the condensate will continues to precipitate in large quantities, and some of the condensate oil may become trapped in pore throats, which will severely damage the gas relative permeability of the formation. On the other hand, if the lower pressure limit is set too high, the gas in the CUGS cannot be produced sufficiently. Therefore, a reasonable lower pressure limit needs to be determined to balance the CUGS capacity and efficiency.

3. Methodology

3.1. Model description

The compositional simulator in t-Navigator 2021.4 was utilized to simulate both the depletion and the CUGS development stage. Table 1 shows the details of the numerical simulation model properties. Three scenarios were simulated in this research: (1) a 19-year depletion development phase with a high-precision history matching rate to verify the accuracy of the conventional model; (2) six rounds of CUGS injection and production simulations conducted using both the standard pseudo-component model and the dynamic pseudo-component model; and (3) five rounds of CUGS operation simulations carried out using the dynamic pseudo-component model to determine the optimal lower pressure limit. This dynamic pseudo-component model can dynamically adjust according to the composition of the injected natural gas. The next section will explain the specific techniques in detail.

The raw data used for numerical simulation in this research were obtained from seismic interpretation results and production logging. The accuracies of these data are usually 1 m and 0.125 m, respectively. Due to the extensive size of the reservoir, reaching 7.2 km^2, a slight coarsening of the geological model was performed to improve the computational speed and reduce the possibility of non-convergence. Consequently, the final model comprised over ten million grids, featuring grid dimensions of 212 × 503 × 95. The model's horizontal resolution is set at 15 m, while the vertical resolution is 0.4 m. This degree of grid precision ensures that the model can accurately depict geological information.

For large-scale real reservoir simulation tasks, a history matching process is necessary, where the model parameters are iteratively adjusted to match the actual production data. This process may require hundreds of runs of the model, and if the model computations are slow, the history matching work becomes almost impossible to complete, rendering the previously constructed fine geological model meaningless. Therefore, for this realistic model, the convergence difficulty and computation time of the model become crucial considerations. Since phase equilibrium calculations are required for each component within every grid cell, they take up most of the computation time for numerical simulation processes. Consequently, having more components in the model leads to longer a calculation time. To reduce the phase balance computational burden caused by ten million grids, a simplified model with seven pseudo-components was introduced in this research.

3.2. Dynamic pseudo-component simulation workflow

The traditional simulation workflow for pseudo-components is illustrated in Fig. 5(a). The process commences by fitting fluid properties using phase behavior experiments, e.g., constant composition expansion (CCE) and constant volume depletion (CVD). Through these experiments, the thermodynamic properties of each pseudo-component are ascertained, including its critical temperature, critical pressure, and acentric factor. The model employs these constant thermodynamic properties to compute properties for each grid and each step, namely, viscosity, volume coefficients, and others [33]. Subsequently, it identifies the lower pressure limit based on the model's production performance. Consequently, in the traditional simulation workflow, the thermodynamic properties of each pseudo-component are kept constant, with only the mole fractions being adjusted at every step.

However, the diversity of thermodynamic properties during the CUGS stage becomes more complex when natural gas is injected, leading to extensive mixing with pre-existing condensate components. Consequently, the thermodynamic properties of the pseudo-components undergo changes, making the previously determined phase equilibrium parameters insufficient. To address this, our study introduces a workflow depicted in Fig. 5(b) for the dynamic pseudo-component model, ensuring an accurate simulation of the phase change process in CUGS.

With the comparison in Fig. 5, it is evident that the dynamic pseudo-components simulation workflow was established based on the foundation of CCE and CVD experimental results. Compared to traditional methods, this approach incorporates multiple experiments, thus increasing the complexity of the simulation process. However, for the development of a large-scale CUGS facility, the initial investment may reach hundred million dollars. Integrating the traditional process with these experiments is both essential and efficient, as the dynamic model enhances the accuracy of the equilibrium calculation processes, facilitating a precise assessment of condensate oil variations.

3.2.1. Constructing the initial pseudo-component model

To create an accurate model, the initial pseudo-component model should be developed into a seven-pseudo-components model (CO_2, N_2, C1, C2–C3, C4–C6, C7–C10, C11+), which is adjusted to match relative volumes, bubble point pressure, dew point pressure, and the dissolved gas-oil ratio based on CCE and CVD test results [40,41]. Additionally, the seven-pseudo-components model should be utilized for numerical simulation and matched with historical production data, including gas, condensate oil, and water production rates, and pressure changes. Once the correlation ratio attains 90 %, the numerical model can be considered reliable for further analysis and informed decision-making.

3.2.2. Determining the dynamic pseudo-components properties

To determine a relationship between pseudo-component thermodynamic properties and various volumes of natural gas injection, we tested

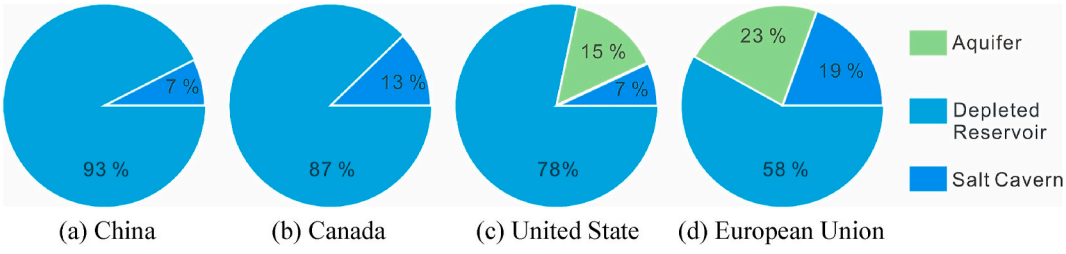

Fig. 2. Percentage of UGS types in different regions.

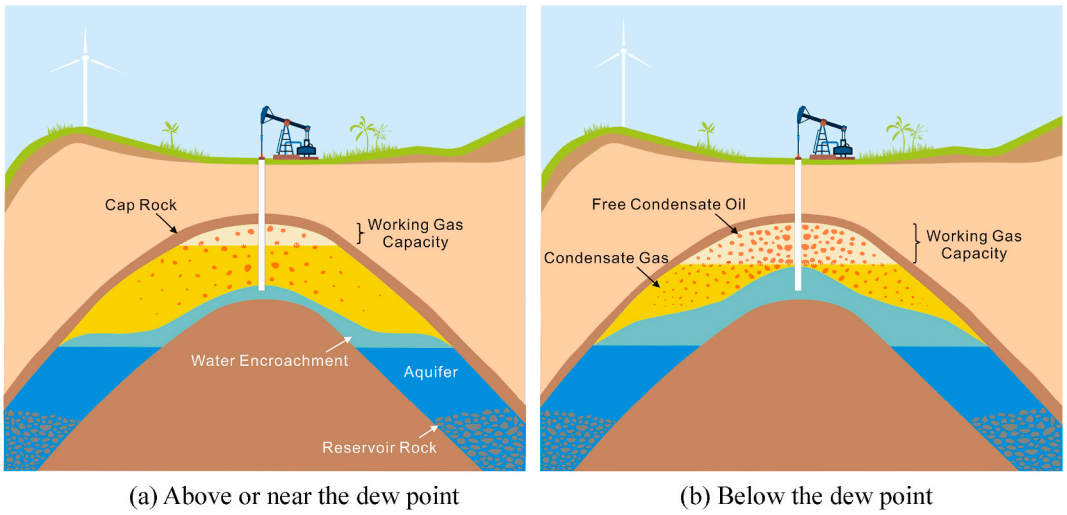

Fig. 3. Comparison of CUGS operating with different lower pressure limit.

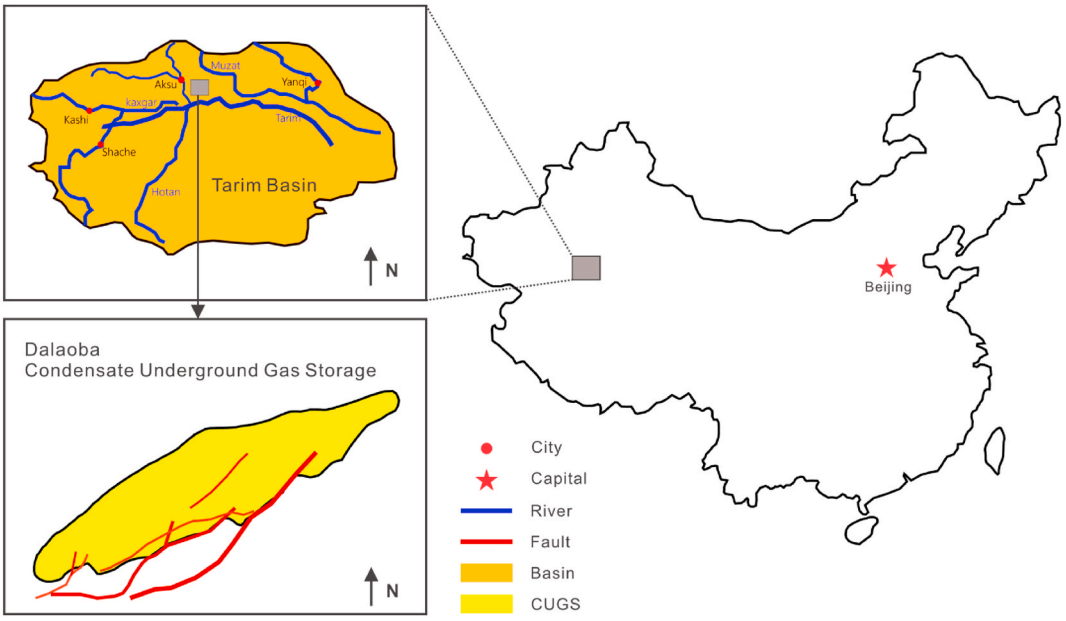

Fig. 4. Tarim Basin and position of Dalaoba CUGS.

Table 1
Basic parameters of the model.

Reservoir Property	Value	Unit
Reservoir Area	7.2	km^2
Depth	4900.0	m
Initial Pressure	57.0	MPa
Thickness	31.9	m
Initial Reservoir Temperature	409.4	K
Average Porosity	17.2	%
Average Permeability	45.3	mD
Rock Compressibility	1.6×10^{-5}	MPa
Gridding Size - I, J, K	$15 \times 15 \times 1$	m
Total Grid Number	1013×10^4	value

four mixed gas samples and one pure natural gas sample. Throughout these tests, each sample's volume remained consistent, with experiments conducted under the prevailing temperature and pressure conditions of the Dalaoba gas reservoir, specifically 409 K and 40 MPa. The volume proportions of natural gas in the mixed samples were 20 %, 40 %, 60 %, and 80 %, respectively, and the pure sample was 100 %. Subsequently, the five samples were to undergo CCE and CVD tests to track changes in their relative volume, bubble point pressure, dew point pressure, and dissolved gas-oil ratio. By employing multiple objective particle swarm optimization techniques, the critical temperature, critical pressure, and acentric factors in the pseudo-components can be adjusted to match the test results of these five samples. Finally, a comprehensive understanding of the relationship between the injected natural gas volumes and the three thermodynamic parameters (critical temperature, critical pressure, and acentric factors) can be established.

3.2.3. *Conducting the dynamic pseudo-components numerical simulation*

After converting the condensate reservoir into a CUGS facility, a dynamic pseudo-component simulation method was implemented. The procedure involves several key steps to ensure accurate results. First, the mole fraction of the injected natural gas in each grid is derived from the component numerical model. This fraction aids in determining the thermodynamic parameters of each pseudo-component, grounded on the previously established thermodynamic property relationships [40,

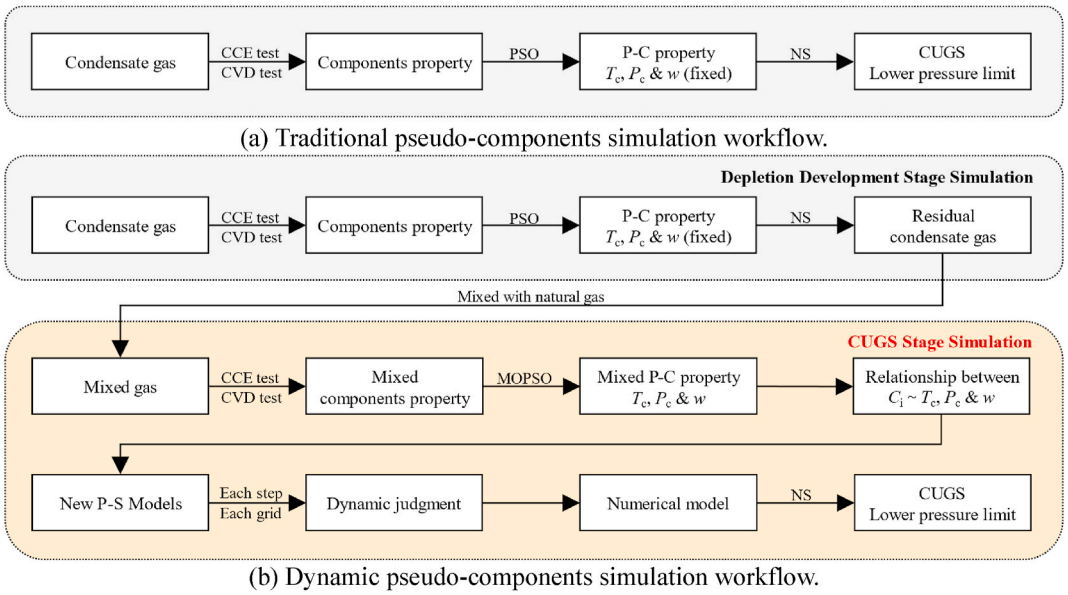

Fig. 5. The workflow for CUGS simulation. P–C: pseudo-components, NS: numerical simulation.

41]. Subsequently, phase balance calculations are conducted using the updated pseudo-component properties. This step enables the determination of fluid properties, such as viscosity and a volume coefficient. Once this calculation is complete, the process is repeated in the next time step, until the completion of the simulation process concludes.

3.3. Governing equations

The dynamic pseudo-component simulation process depends on several factors, including the timely updating of molar weight, critical temperature, critical pressure, and acentric factor at each computational time step. In the numerical simulation process, the molar weight of each pseudo-component can be accurately determined using the component numerical model, as described in Section 3.3.1. The thermodynamic properties were then derived by regressing multiple experimental test results using the multiple objective particle swarm optimization (MOPSO) method, detailed in Section 3.3.2. Furthermore, the Peng-Robinson equation of state (PR-EOS), discussed in Section 3.3.3, is employed to calculate the fluid properties with the obtained dynamic thermodynamic properties. The detailed equations are outlined below.

3.3.1. Component numerical model

In the compositional numerical model, there are three types of governing equations: mass conservation for each component, Darcy's equation, and the equation of state (EOS). These equations are interconnected as follows [40–42].

The governing mass conservation equations for each component can be expressed as Eqs. (1) and (2):

Water component:

$$-\nabla\cdot(\xi_w u_w)=\frac{\partial}{\partial t}(\varphi s_w \xi_w)+Q_w \tag{1}$$

i-th component:

$$-\nabla\cdot\left(x_i\xi_o u_o+y_i\xi_g u_g\right)=\frac{\partial}{\partial t}\left(\varphi\left(s_o x_i\xi_o+s_g y_i\xi_g\right)\right)+Q_i \tag{2}$$

where ξ_w, ξ_o and ξ_g is the molar density of each phase, which can be obtained from Eqs. (3)–(5):

Water phase:

$$\xi_w=\frac{\rho_w}{M_w} \tag{3}$$

Oil phase:

$$\xi_o=\frac{\rho_o}{\sum_{i=1}^{n_c}x_i M_i} \tag{4}$$

Gas phase:

$$\xi_g=\frac{\rho_g}{\sum_{i=1}^{n_c}y_i M_i} \tag{5}$$

where u_j is the velocity of each phase, including water, oil, and gas, can be solved by following Darcy's equation:

$$u_j=-\frac{kk_{rj}}{\mu_j}\cdot\left[\nabla p_j-10^{-6}\rho_j g\nabla Z\right] \tag{6}$$

The equation of state (EOS) approach is utilized to represent instantaneous thermodynamic phase equilibrium according to the principle of equal fugacity in liquid and gas phases:

$$f_{i,l}(p,T,x_1,x_2,\cdots,x_{nc})=f_{i,g}(p,T,y_1,y_2,\cdots,y_{nc}) \tag{7}$$

Additional linear constraints are imposed on the component phase compositions and phase saturations, as follows.

$$\sum_{i=1}^{n_c}x_i=1 \tag{8}$$

$$\sum_{i=1}^{n_c}y_i=1 \tag{9}$$

Water, oil and gas phase:

$$s_w+s_o+s_g=1 \tag{10}$$

The above equations characterize the multiphase compositional model, in which subscripts w, o and g represent the water, oil and gas phase, respectively; subscripts i represent different components; subscripts j signifies distinct phases; Q is an injected or produced flow rate [m^3/s]; u is the Darcy velocity [m/s]; φ is the rock porosity [unitless]; s is the fluids saturation [unitless]. ρ is the mass density [kg/m^3]; g is the gravitational acceleration [9.8 m/s^2]; M is the molar weight [kg/mol]; $f_{l,i}$ and $f_{g,i}$ are the fugacities of the i-th component in the liquid and gas phase, respectively [unitless]; x_i and y_i respectively represent mole fractions of the i-th component in the liquid and gas phase [unitless]; μ is

the fluid viscosity [cP]; k is the rock permeability [mD]; k_r is the relatively permeability [unitless]; p is the fluid pressure [MPa]; T is the reservoir absolute temperature [K].

3.3.2. Multiple objective particle swarm optimization

Coello proposed a MOPSO method, which has the advantage of optimizing multiple objectives within the same convergence system [43]. In the study of the dynamic pseudo-component model, the thermodynamic properties, including the critical pressure, critical temperature, and acentric factor, were obtained by fitting CCE and CVD experimental results of the five samples with different natural gas fractions. Consequently, Eqs. (11) and (12) serve to calculate the regressed properties of the pseudo-component across distinct natural gas fractions.

$$VEL_i = W \times VEL_i + R_1 \times \left(P_{best,i} - POP_i\right) + R_2 \times \left(REP_h - POP_i\right) \tag{11}$$

$$POP_i = POP_i + VEL_i \tag{12}$$

where W is an inertia weight [unitless] and takes a value of 0.4; R_1 and R_2 are random numbers in the range of [0,1]; $P_{\text{best,i}}$ is the best position that particle i has had; $G_{\text{best,i}}$ is the best position that group i has had; REP_{h} is a value that is taken from a repository; h is the index selected from the standard MOPSO calculation process; VEL_{i} is the speed of particle i; POP_{i} is the current value of particle i.

3.3.3. Fluid model

The PR-EOS is a well-established method for predicting phase parameters across various temperatures and pressures. Although the PR-EOS has been employed in the industry for an extended period, its long-standing application further attests to its effectiveness. The PR-EOS boasts several advantages: its parameters are defined by critical and acentric factors, most of which are exclusively related to temperature, pressure, and composition. Moreover, the PR-EOS can achieve remarkable accuracy near a critical state, especially for compression factor and fluid density calculations [44–46]. Because of its effectiveness in gas-liquid two-phase equilibrium calculations, the PR-EOS is widely embraced by the petroleum industry. In light of these benefits, our phase equilibrium discussion will employ the PR-EOS.

The PR-EOS for multi-component hydrocarbon systems is as follows:

$$P = \frac{1305.3390RT}{0.1419V - 5b_m} - \frac{145.0377(a\alpha)_m}{0.0008V^2 + 0.0567b_mV - {b_m}^2} \tag{13}$$

where V is the molar volume [m^3/lbmol]. The mixture parameters, $(a\alpha)_m$ and b_m are determined as functions of the properties of the individual components, using the following mixing rules:

$$(a\alpha)_m = \sum_i^{n_c}\sum_j^{n_c} c_i c_j \sqrt{(a\alpha)_i (a\alpha)_j}\left(1 - \delta_{ij}\right) \tag{14}$$

$$b_m = \sum_i^{n_c} c_i b_i \tag{15}$$

where δ_{ij} is binary interaction coefficient between the i-th and j-th components, symmetric in i and j with $\delta_{ii} = 0$; c is the molar composition [%] and the sum of the molar compositions of all components is 100 %; $(a\alpha)_i$ is dimensional attraction parameter for the i-th component in the mixture fluids; b_i is the dimensional co-volume parameters for the i-th component in the mixture, which can be calculated using Eqs. (16) and (18).

$$(a\alpha)_i = 469.90\frac{R^2T_{ci}^2}{p_{ci}}\left[1 + m_i\left(1 - T_{ri}^{0.5}\right)\right]^2 \tag{16}$$

$$b_i = 261.05\frac{RT_{ci}}{p_{ci}} \tag{17}$$

$$m_i = \begin{cases} 0.3746 + 1.5423\omega_i - 0.2699\omega_i^2 & (\omega_i \le 0.49) \\ 0.3796 + 1.4851\omega_i - 0.1644\omega_i^2 + 0.017\omega_i^3 & (\omega_i > 0.49) \end{cases} \tag{18}$$

where T_{ci} is the absolute critical temperature of the i-th component [K]; T_{ri} is the reduced temperature, which is the ratio of the sample's temperature to the critical temperature [unitless]; p_{ci} is the critical pressure of the i-th component [MPa]. ω_i is Pitzer's acentric factor [unitless]; R is the universal gas constant [8.314×10^{-6} MPa m^3/mol·K].

4. Result and discussion

In order to demonstrate the entire process of determining the lower pressure limit for CUGS, the dynamic pseudo-component simulation method was employed on an example system. This example involves the establishment of a pseudo-component model with seven components using the K-means clustering method. Subsequently, a dynamic pseudo-component model for the Dalaoba CUGS is constructed. The dynamic pseudo-component model was then used to predict the condensate oil production rate. Finally, using the calibrated dynamic model, a total of five cycle cases were conducted to determine the lower pressure limit for Dalaoba CUGS.

4.1. Dynamic pseudo-component model establishment

4.1.1. Pseudo-components lumping rule

The criteria for lumping pseudo-components are based on the varying thermodynamic properties of the individual components. Due to the distinct thermodynamic properties of carbon dioxide and nitrogen, combined with their notable molar compositions of 0.83 % and 3.04 % in the Dalaoba condensate reservoir, they are not typically lumped into a single pseudo-component. C11+ is an aggregation of all components which cannot be accurately measured and should be treated as an independent pseudo-component. To determine other pseudo-component lumping schemes, the K-means clustering analysis technique is employed by utilizing Eq. (19) for the acentric factors, as it serves as an indicator of the curvature associated with the pure component vapor pressure curve. The classification results are presented in Table 2, where pseudo-component 1 represents C2–C3, pseudo-component 2 represents C4–C6, pseudo-component 3 represents C7–C10, and pseudo-component 4 represents C11+.

$$J = \sum_{j=1}^{k}\sum_{i=1}^{n}\left\|x_i - a_j\right\|^2 \tag{19}$$

where J is the objective function, $||\ x_i - a_j\ ||$ is the Euclidean distance between the data point x_i and the cluster center a_j, k is the number of

Table 2
Pseudo-components lumping scheme.

Component	Acentric factor	K-means cluster center	Lumping scheme
N_2	0.038	0.038	Component 1 (N_2)
CO_2	0.228	0.228	Component 2 (CO_2)
C1	0.012	0.012	Component 3 (C1)
C2	0.100	0.126	Pseudo-component 1
C3	0.152		(C2–C3)
IC4	0.184	0.223	Pseudo-component 2
NC4	0.200		(C4–C6)
IC5	0.228		
NC5	0.252		
C6	0.250		
C7	0.280	0.331	Pseudo-component 3
C8	0.312		(C7–C10)
C9	0.348		
C10	0.385		
C11+	0.662	0.662	Pseudo-component 4 (C11+)

clusters, and n is the number of cases.

4.1.2. Pseudo-components thermodynamic properties

Lee proposed a static sample component regrouping model that utilized mixing rules as the characterizing approach to determine the thermodynamic properties of the pseudo-component [47]. First, we calculate a lumped fraction according to Eq. (20), and then compute the pseudo-components' critical temperature, critical pressure, and acentric factor using Eqs. (21)–(23), respectively.

$$z_i^* = \frac{z_i}{\sum_{i\in L}^{L} z_i} \tag{20}$$

$$p_c = \sum_{i\in L}^{L} \left(z_i^* p_{ci}\right) \tag{21}$$

$$T_c = \sum_{i\in L}^{L} \left(z_i^* T_{ci}\right) \tag{22}$$

$$\omega_c = \sum_{i\in L}^{L} \left(z_i^* \omega_{ci}\right) \tag{23}$$

where z_i is the mole fraction of component i [unitless]; L is a collection of regrouping components; z_i^* the pseudo-component lumped fraction [unitless]; T_c is the pseudo-component critical temperature [k]; P_c is the pseudo-component critical pressure [MPa]; ω_c is the pseudo-component acentric factor [unitless].

4.1.3. Dynamic pseudo-component model

By utilizing MOPSO, the uncertain thermodynamic parameters of pseudo-component 1–4 are determined. Fig. 6(a) to 6(c) represent the pseudo-component's critical temperature, critical pressure, and acentric factor across different natural gas contents. Moreover, Fig. 6(d) illustrates the relative change of pseudo-component within the range of HCPV from 0 to 1. As natural gas is gradually introduced, the thermodynamic properties of pseudo-component begin to change noticeably. Specifically, the critical temperature and acentric factors decrease, while the critical pressure increases significantly. These changes become even more noticeable as the amount of natural gas injected increases. Nonetheless, the data also indicates that different pseudo-components exhibit different changing trends. For lighter components below C7, the changes in the three properties are relatively minor, with differences of no more than 18 %. In contrast, heavier components above C7 experience substantial changes, with the critical pressure being the most affected property, sometimes increasing by up to 133 %.

Fig. 7 illustrates the phase behavior of pseudo-component under different injection volumes. In Fig. 7(a), as the volume of injected natural gas increases, the envelope line consistently contracts, with the critical condensation pressure decreasing from 51 MPa to 32 MPa. At the Dalaoba CUGS formation temperature of 409K, the dew point pressure is around 28 MPa with original condensate gas. However, during production, when the temperature drops to the surface temperature of 298K, the dew point pressure decreases from 46 MPa to 17 MPa with a 40 % natural gas mixture. A 60 % mixture is sufficient to prevent condensate oil precipitation. The change in the equilibrium constant during the phase equilibrium calculation process can represent the

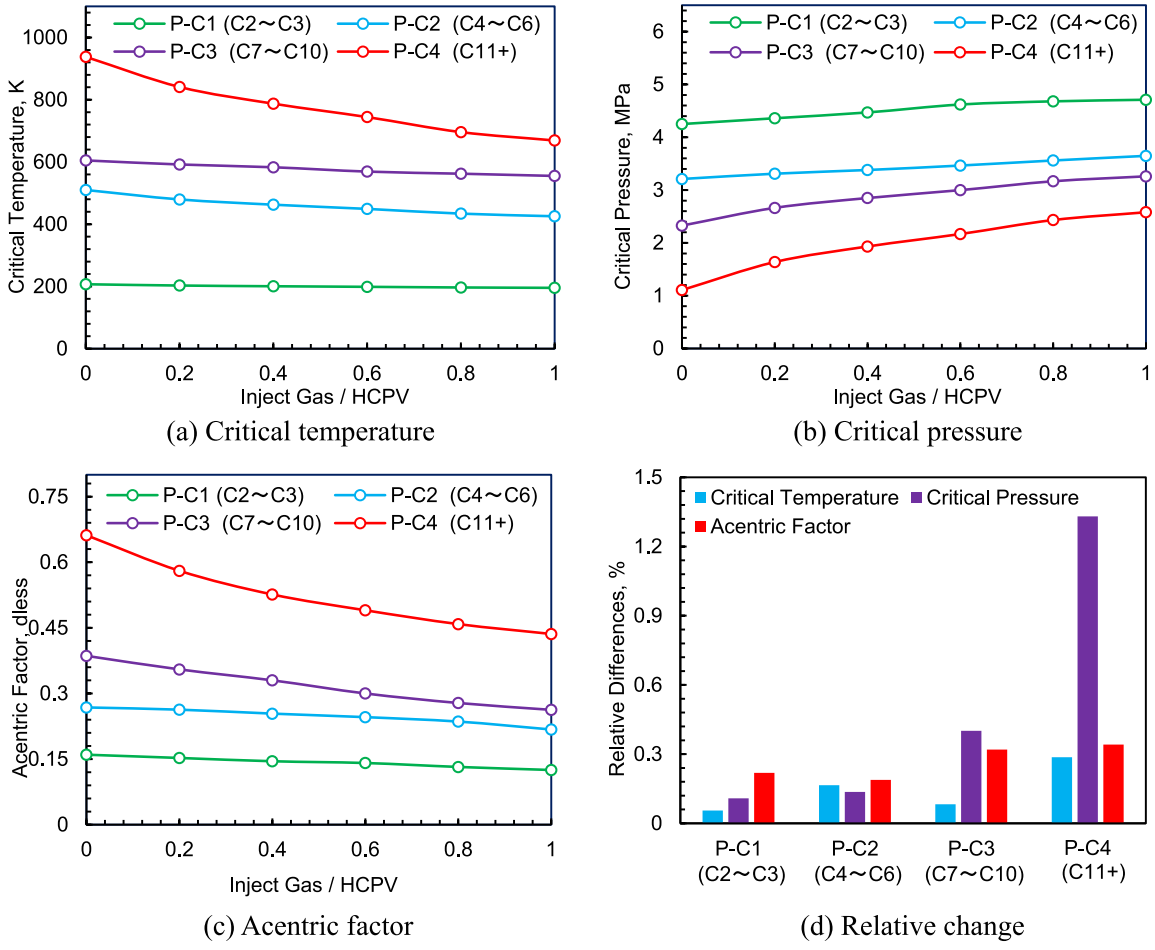

Fig. 6. Pseudo-component thermodynamic properties (P–C: Pseudo-component).

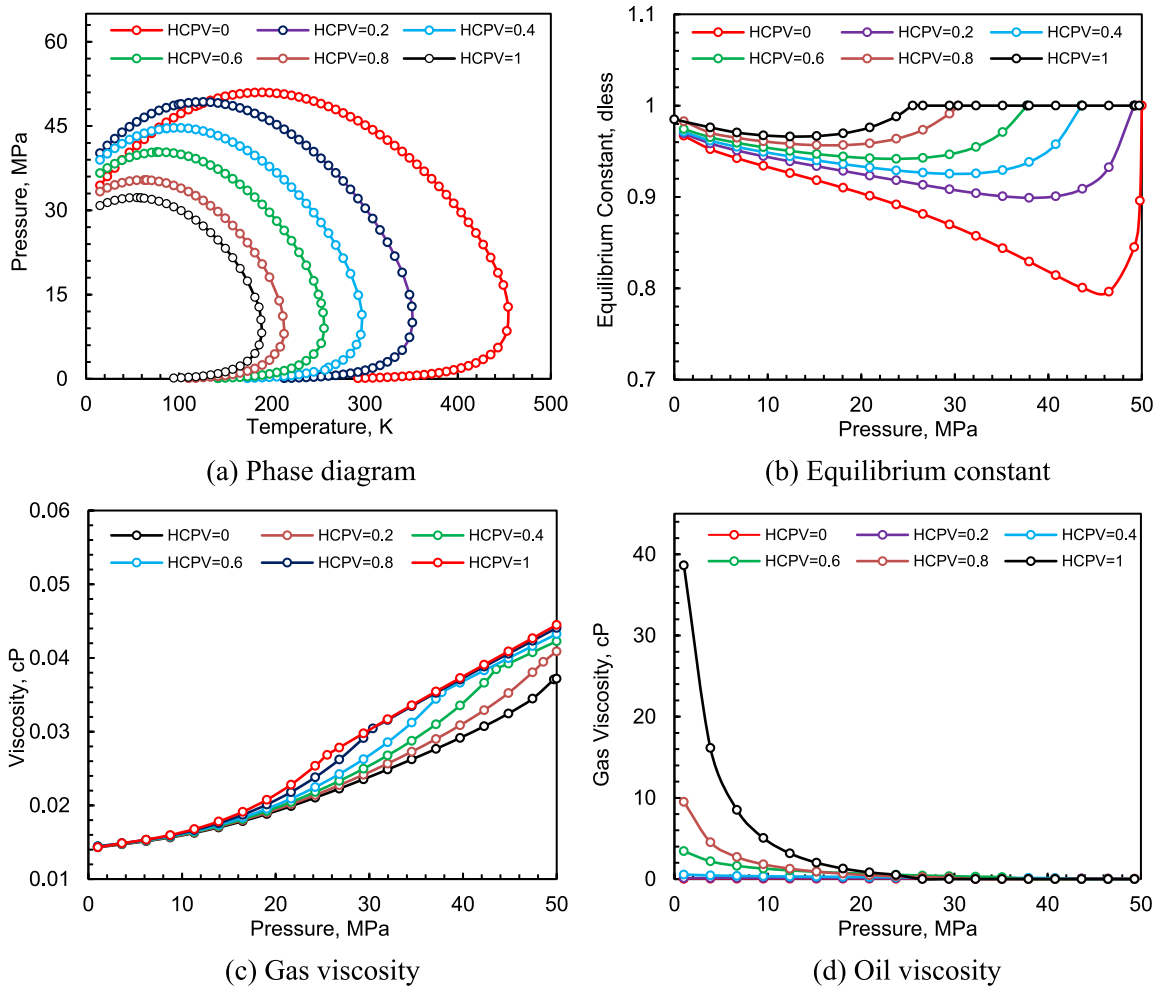

Fig. 7. Dynamic pseudo-component property changes.

precipitation rate of condensate oil. Fig. 7(b) shows that in the early stage of CUGS gas injection, the precipitation rate of condensate oil is fast, and subsequently gradually slows down. Once the injection surpasses 0.4 PV, the precipitation rate stabilizes at a reduced level. Fig. 7 (c) illustrates the variations in the gas viscosity, which rises when the pressure exceeds 20 MPa, suggesting a gradual decline in the gas flow capacity as the CUGS develops. This range of fluctuations is approximately within 27 %. Lastly, Fig. 7(d) displays the variations in the condensate oil viscosity, which remains nearly constant above 20 MPa. However, since the operating pressure for the CUGS is generally not set so low, a change in the condensate oil viscosity has little impact on CUGS.

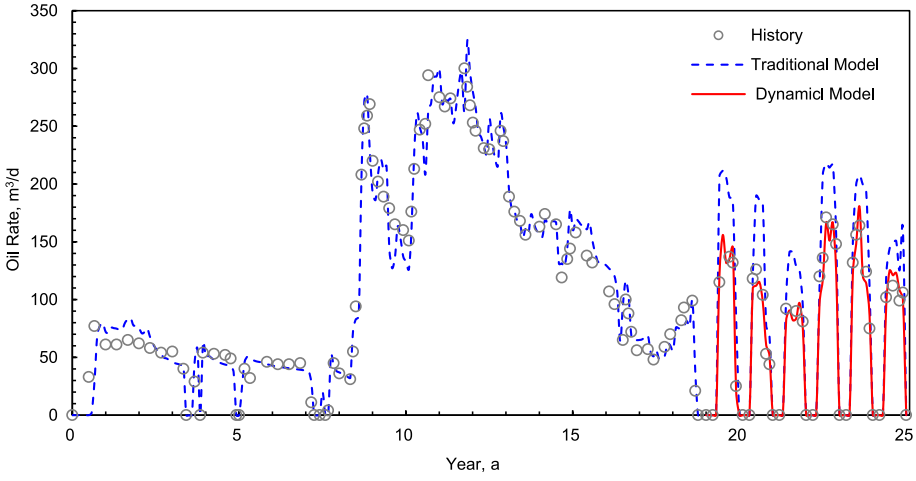

Fig. 8. Historical data and two simulation models for condensate oil production rate.

4.2. Dynamic pseudo-component history matching

The Dalaoba CUGS, established in a condensate gas reservoir, presents a 25-year production and injection history, as illustrated in Fig. 8. The first 19 years are marked by the depletion development stage, followed by a 6-year CUGS construction phase that includes six injection and production cycles. In consideration of the geological characteristics and reservoir engineering principles, we have performed multiple adjustments to a traditional numerical model for the Dalaoba condensate gas reservoir, including modifying relative permeability, rock properties, and fault characteristics. These adjustments enable the model to effectively capture the actual seepage during the depletion stage. As demonstrated in Fig. 8, the historical data, denoted by gray dots, closely aligns with the blue dashed line representing the traditional model throughout the initial 19 years. However, during the CUGS phase which began in the 20th year, it was noticed that the traditional model overestimated the amount of condensate oil in each production cycle when contrasted with the actual historical data.

As previously stated, this primarily stemmed from the substantial injection of natural gas into the formation following the conversion of the gas reservoir into the CUGS, leading to a pronounced alteration in the thermodynamic properties of the underground hydrocarbon substances. The traditional model continued to use the original pseudo-component properties, leading to its inability to reflect the actual underground conditions. In contrast, by applying the dynamic pseudo-component model introduced earlier during the CUGS phase, a satisfactory fit is achieved, as illustrated by the red curve in Fig. 8. This suggests that the dynamic component model can effectively simulate phase balance behavior during the gas injection phase and accurately represent the actual subsurface conditions.

4.3. Lower pressure limit determination

The lower pressure limit is a crucial parameter in the operation of UGS. An inaccurate lower pressure limit may result in significant water intrusion into the reservoir, which is the major concern for UGS. Several key reference indicators are currently employed, such as reservoir capacity, a water intrusion volume, and gas storage production capacity [26,48–50]. For CUGS, alterations in the lower pressure limit can impact the condensate oil content, which affects the flow capacity of the formation in return. This study takes into account factors like retrograde condensation, gas flow capacity, and water encroachment.

4.3.1. Retrograde condensation

In the dynamic pseudo-component simulation process, the gas-liquid ratio of each component under the corresponding temperature and pressure conditions can be calculated according to Eqs. (24) and (25), which determine the amount of free condensate oil produced due to the retrograde condensation process:

$$x_i = \frac{c_i}{1 + f_{ng}(K_i - 1)} \tag{24}$$

$$V_o = \sum_{1}^{n_c} x_i V_b \varphi \tag{25}$$

where f_{ng} is the vapor/liquid molar fraction [unitless]; K_i is the equilibrium constants [unitless]; V_b is the volume of grid cell [m^3]; V_o is the free condensate oil volume [m^3].

Fig. 9 illustrates the oil saturation at the end of the five rounds of the Dalaoba CUGS production cycles using the dynamic pseudo-component simulation model. As illustrated in Fig. 9(a), some regions may still contain condensate even when the pressure returns to its original level due to reservoir heterogeneity, particularly in areas with low permeability. Fig. 9(a) to 9(d) indicate a substantial increase in oil saturation as pressure declines, especially when the pressure falls below 35 MPa.

Fig. 10 displays a correlation between the volume of free condensate oil and reservoir pressure in the Dalaoba CUGS. The volume of free condensate oil evidently increases exponentially as the reservoir pressure declines. The regression analysis indicates that the turning point is at 41 MPa. This signifies that when the CUGS pressure drops below this value, free condensate oil is generated at a fast pace, causing disturbances to the reservoir's flow environment. The turning pressure of the free condensate oil volume provides an important reference for setting the minimum operating pressure for the CUGS.

4.3.2. Gas flow capacity

Using the dynamic pseudo-compositional model, five cycles of gas injection and production analyses were conducted within a lower pressure range of 35 MPa–47 MPa. Each cycle involved gas injection for six months with a volume of 58×10^6 m^3, followed by a production stage of six months with a fixed gas production rate of 32×10^4 m^3/d. The variations in gas and water production were plotted against different lower pressure targets, as shown in Fig. 11. The following observations can be made from the study: (1) The CUGS's gas production capacity improves with escalating production cycles within a constant lower pressure target, which means the CUGS's flow environment will

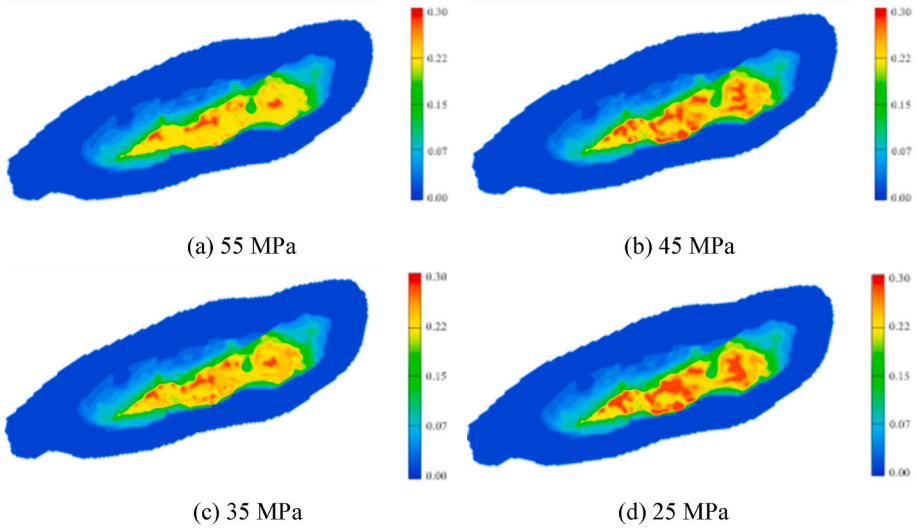

Fig. 9. The oil saturation with different lower pressure limits.

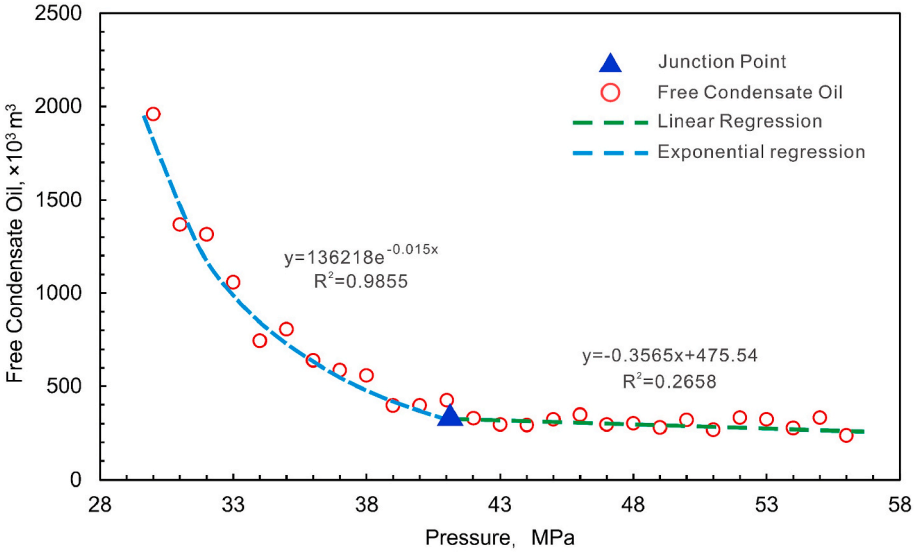

Fig. 10. The total volume of free condensate oil with different lower pressure limits.

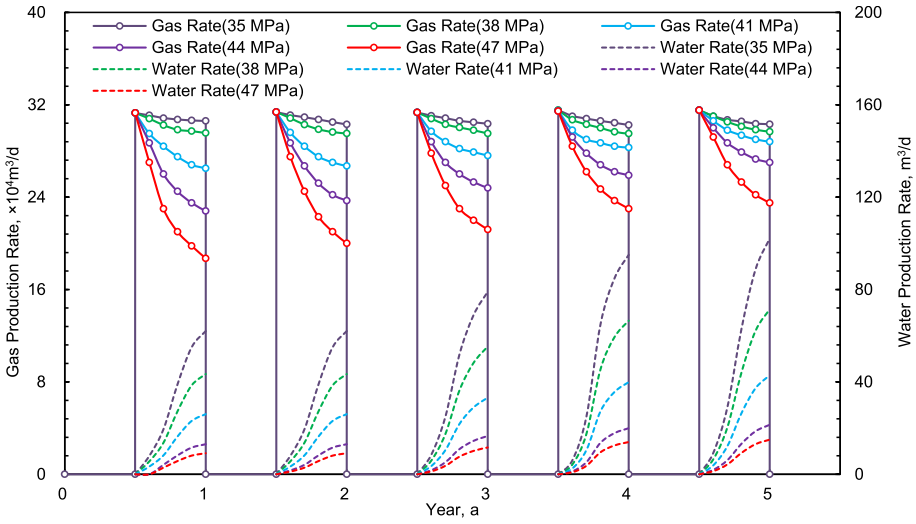

Fig. 11. Gas and water production rate with different lower pressure limits.

gradually improve with the natural gas injection. (2) Setting a higher lower pressure limit target resulted in a reduced water production rate in the CUGS, but it also led to a decrease in the gas supply capacity. For example, when the lower pressure limit was set at 47 MPa, there was a decline in the gas production rate of up to 40.2 %. Since the lower pressure limit is the target pressure set for production wells, a higher pressure limit indicates a smaller production pressure drop and a reduction in production capacity. (3) Conversely, a significantly lower pressure limit target boosted the gas supply capacity but led to a substantial rise in the water production rate. For example, when the lower pressure limit was set at 35 MPa, the maximum water production reached 103 m^3/d. This made surface dehydration more challenging and suggested that significant water encroachment had occurred under the CUGS formation. (4) Considering the need for a stable gas supply and minimized water production, the lower pressure limit for the Dalaoba CUGS should be maintained at approximately 41 MPa. At this pressure, the daily gas supply should be no less than 25 × 104 m^3/d.

4.3.3. Water encroachment

An additional critical factor linked to the CUGS's lower pressure limit is water encroachment. As the pressure target decreases, there's a general increase in the volume of aquifer influx, adversely affecting the effective storage capacity of the CUGS. Therefore, maintaining the lower pressure limit to protect the reservoir from large-scale water encroachment is a crucial consideration. Fig. 12 demonstrates the variations in the water encroachment volume in CUGS at distinct lower pressure limits. The volume increases rapidly as the pressure target decreases, especially when the pressure drops below 41 MPa. With the same lower pressure limit target, the water encroachment volume grows as more cycles are conducted, and this growth range is more pronounced at a higher pressure target. For example, with lower pressure limits set at 47 MPa and 35 MPa, the difference in the water encroachment volume between the first and fifth cycles are 19.5 % and 3.3 %, respectively. This phenomenon can be attributed to variations in the capillary force in wet rocks, which complicates the displacement of water from the layer following a water influx.

4.4. Industrial application scenarios

This study introduces a dynamic pseudo-component model for calculating the Lower Pressure Limit of the Dalaoba CUGS. The described dynamic simulation methods and technical processes are

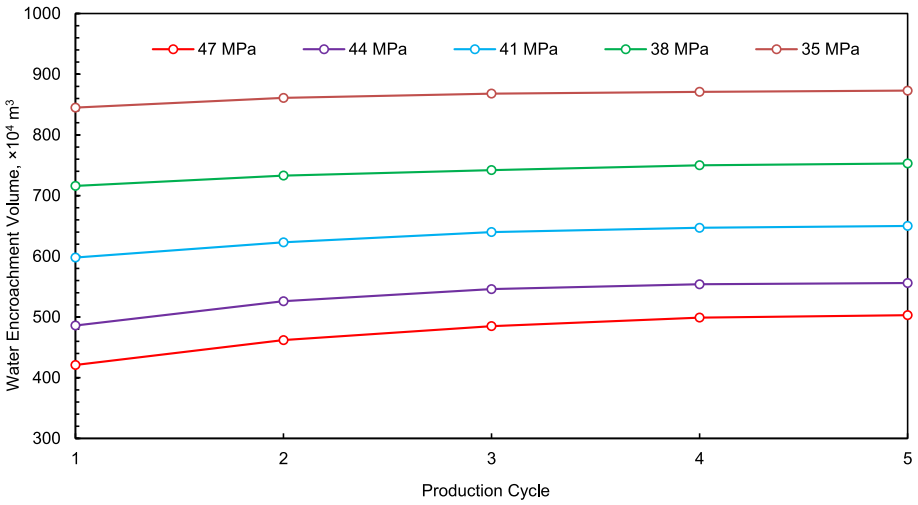

Fig. 12. Water encroachment volumes with different lower pressure limits.

applicable to diverse industrial Application scenarios.

(1) The dynamic pseudo-component model: This model is beneficial for optimizing parameters related to condensate gas reservoirs development through natural gas injection. It also helps in simulating CUGS performance under various production systems and improves recovery rates through natural gas injection in oil reservoirs. In these industrial application scenarios, large-scale natural gas injection alters the thermodynamic properties of the reservoir's original fluids. By utilizing the dynamic pseudo-component model, accurate thermodynamic properties can be obtained in real-time, and precise phase equilibrium calculations can be conducted.
(2) The calculation workflow for determining the lower pressure limit of gas storage: This approach is applicable to various gas storage types, including traditional sandstone gas and oil reservoir UGS, condensate gas reservoir UGS, and aquifer UGS. This study establishes methodologies for parameters such as condensate oil yield, gas production capacity, and a water encroachment volume. These methodologies are also applicable to other gas storage facilities.

5. Conclusions

This paper introduces a dynamic pseudo-component model that employs a million-grid scale to simulate a CUGS facility converted from a condensate gas reservoir. Taking into account factors like condensate oil production, gas flow capacity, and water encroachment, the research offers recommendations for determining the lower pressure limit for the CUGS. The main conclusions reached are as follows.

(1) A dynamic pseudo-component model has been introduced. While this model increases the workload and necessitates five additional sets of experiments, it overcomes the limitations of traditional models that rely on constant thermodynamic properties. In the numerical simulation process, the model dynamically updates thermodynamic parameters based on the volume of the injected natural gas. This approach provides an accurate representation of condensate gas properties when they are diluted with injected natural gas and enables more precise phase equilibrium calculations. Consequently, the accuracy of condensate oil production calculations is enhanced after substantial natural gas injection.
(2) The dynamic pseudo-component model is suitable for large-scale natural gas injections in condensate gas reservoirs. This model facilitates the conversion of depleted condensate reservoirs to CUGS and aids in maintaining pressure during the development of such reservoirs. The dynamic pseudo-component model is based on CCE and CVD experiments that involve the mixing of condensate gas and natural gas samples, which accurately determine a relationship between thermodynamic properties and the volume of the mixed gas.
(3) Converting abandoned condensate gas reservoirs into CUGS facilities allows for the restoration of reservoir pressure through multiple gas injection cycles. Additionally, during the gas production stage, there is continuous dilution of the heavy component content in the reservoir. Both aspects contribute to enhancing the reservoir's flow environment during the CUGS phase.
(4) The lower pressure limit for a CUGS facility is a vital operational parameter that influences gas production stability, a condensate oil production volume, and water encroachment into the formation. In practice, the interplay among these three factors often leads to conflicts, necessitating the use of numerical simulation methods to ascertain and set an optimal value for the lower pressure limit.

CRediT authorship contribution statement

Peng Deng: Conceptualization, Investigation, Methodology, Writing - original draft, Writing - review & editing. **Zhangxin Chen:** Methodology, Funding acquisition, Supervision. **Xiaolong Peng:** Writing – review & editing, Supervision. **Jianfeng Wang:** Investigation, Data curation. **Suyang Zhu:** Methodology, Data curation. **Haoming Ma:** Validation, Writing – review & editing. **Zhengbin Wu:** Validation, Formal analysis.

Declaration of competing interest

The authors declare that they have no known competing financial interests or personal relationships that could have appeared to influence the work reported in this paper.

Data availability

Data will be made available on request.

Acknowledgements

This research has been made possible by contributions from the Natural Sciences and Engineering Research Council (NSERC)/Energi

Simulation Industrial Research Chair in Reservoir Simulation, the Alberta Innovates (iCore) Chair in Reservoir Modeling, the Energi Simulation/Frank and Sarsh Meyer Collaboration Centre. Open Fund for PetroChina's Key Laboratory of Fractured Reservoirs Enhanced Oil Recovery[grant number 34400000-22-ZC0607-0004]. "Central Government Guides Local Science and Technology Development" in Sichuan Provincial Department of Science and Technology [grant number 2022ZYD0003].

References

[1] IEA. World. Energy outlook 2022. 2022. Paris.
[2] Lankof L, Urbańczyk K, Tarkowski R. Assessment of the potential for underground hydrogen storage in salt domes. Renew Sustain Energy Rev 2022;160:112309.
[3] Caglayan DG, Weber N, Heinrichs HU, Linben J, Robinius M, Kukla PA, et al. Technical potential of salt caverns for hydrogen storage in Europe. Int J Hydrogen Energy 2020;45:6793–805.
[4] Małachowska A, Łukasik N, Mioduska J, Gębicki J. Hydrogen storage in geological formations—the potential of salt caverns. Energies 2022;15:5038.
[5] Zhang GX, Li B, Zheng DW, Ding GS, Wei H, Qian PS, et al. Challenges to and proposals for underground gas storage (UGS) business in China. Nat Gas Ind B 2017;4:231–7.
[6] Bankes N, Gaunce J. Natural gas storage regimes in Canada: a survey. University of Calgary, Institute for Sustainable Energy, Environment and Economy; 2009.
[7] Lackey G, Freeman GM, Buscheck TA, Haeri F, White JA, Huerta N, et al. Characterizing hydrogen storage potential in US underground gas storage facilities. Geophys Res Lett 2023;50:e2022GL101420.
[8] Tang K, Liao XW, Min ZS, Li B, Zhao GG, Mahlalela BM, et al. Experimental investigation of phase behavior of condensate gas and crude oil system in underground gas storage. Lithosphere 2021:2021.
[9] Davarpanah A, Mazarei M, Mirshekari B. A simulation study to enhance the gas production rate by nitrogen replacement in the underground gas storage performance. Energy Rep 2019;5:431–5.
[10] Arfaee MIR, Sola BS. Investigating the effect of fracture–matrix interaction in underground gas storage process at condensate naturally fractured reservoirs. J Nat Gas Sci Eng 2014;19:161–74.
[11] Tand Y, Long KJ, Wang JM, Xu HC, Wang Y, He YW, et al. Change of phase state during multi-cycle injection and production process of condensate gas reservoir based underground gas storage. Petrol Explor Dev 2021;48:395–406.
[12] Rui ZH, Peng F, Ling KG, Chang HW, Chen G, Zhou XY. Investigation into the performance of oil and gas projects. J Nat Gas Sci Eng 2017;38:12–20.
[13] Nasiri Ghiri M, Nasriani HR, Sinaei M, Najibi S, Nasriani E, Parchami H. Gas injection for enhancement of condensate recovery in a gas condensate reservoir. Energy Sources, Part A Recovery, Util Environ Eff 2015;37:799–806.
[14] Guo P, Jing SS, Peng CZ. Technologies and countermeasures for gas recovery enhancement. Nat Gas Ind B 2014;1:96–102.
[15] Fan L, Harris BW, Jamaluddin A, Kamath J, Mott R, Pope GA, et al. Understanding gas condensate reservoirs. Oilfield Rev 2005;17:14–27.
[16] Zhao XL, Rui ZH, Liao XW. Case studies on the CO2 storage and EOR in heterogeneous, highly water-saturated, and extra-low permeability Chinese reservoirs. J Nat Gas Sci Eng 2016;29:275–83.
[17] Song YL, Song ZJ, Hou JR, Wang ZX. Modifying Peng-Robinson equation of state to consider influence of confinement on fluid phase behavior. Carbon Management Technology Conference. CMTC; 2019.
[18] Chen ZX, Huan GR, Ma YL. Computational methods for multiphase flows in porous media. SIAM; 2006.
[19] Azin R, Nasiri A, Entezari J. Underground gas storage in a partially depleted gas reservoir. Oil & Gas Sci Technol Revue de l'IFP. 2008;63:691–703.
[20] Plaat H. Underground gas storage: why and how, vol. 313. Geological Society, London, Special Publications; 2009. p. 25–37.
[21] Ding GS, Wei H. Review on 20 years' UGS construction in China and the prospect. Oil Gas Storage Transp 2020;39:25–31.
[22] Hui G, Chen ZX, Schultz R, Chen SN, Song ZJ, Zhang ZC, et al. Intricate unconventional fracture networks provide fluid diffusion pathways to reactivate pre-existing faults in unconventional reservoirs. Energy 2023:128803.
[23] Zhang NL, Luo ZF, Chen X, Zhao LQ, Zeng XQ, Zhao MR. Investigation of the artificial fracture conductivity of volcanic rocks from permian igneous in the Sichuan Basin, China, with different stimulation method using an experiment approach. J Nat Gas Sci Eng 2021;95:104234.
[24] Hui G, Chen SN, Chen ZX, Gu F. An integrated approach to characterize hydraulic fracturing-induced seismicity in shale reservoirs. J Petrol Sci Eng 2021;196:107624.
[25] Ding GS, Li C, Wang JM, Xu HC, Zheng YL, Wanyan QQ, et al. The status quo and technical development direction of underground gas storages in China. Nat Gas Ind B 2015;2:535–41.
[26] Ma XH, Zheng DW, Shen RC, Wang CY, Luo JH, Sun JC. Key technologies and practice for gas field storage facility construction of complex geological conditions in China. Petrol Explor Dev 2018;45:507–20.
[27] Sadeghi S, Sedaee B. Mechanistic simulation of cushion gas and working gas mixing during underground natural gas storage. J Energy Storage 2022;46:103885.
[28] Wang JM, Shi L, Zhang Y, Zhang K, Li C, Chen XX, et al. Simulation of petroleum phase behavior in injection and production process of underground gas storage in a gas reservoir. Petrol Explor Dev 2022;49:1386–97.
[29] Wang JK, Zhang JL, Xie J, Ding F. Initial gas full-component simulation experiment of Ban-876 underground gas storage. J Nat Gas Sci Eng 2014;18:131–6.
[30] Sutton RP. Fundamental PVT calculations for associated and gas/condensate natural-gas systems. SPE Reservoir Eval Eng 2007;10:270–84.
[31] Chen ZX. Reservoir simulation: mathematical techniques in oil recovery. SIAM; 2007.
[32] Rahimzadeh A, Bazargan M, Darvishi R, Mohammadi AH. Condensate blockage study in gas condensate reservoir. J Nat Gas Sci Eng 2016;33:634–43.
[33] Ahmed T. Equations of state and PVT analysis. Elsevier; 2013.
[34] Song YL, Song ZJ, Guo J, Feng D, Chang XY. Phase behavior and miscibility of CO2–hydrocarbon mixtures in shale nanopores. Ind Eng Chem Res 2021;60:5300–9.
[35] Tien CM, Lin HW, Chen JF, Wu WJ. Case study of underground gas storage in a lean gas condensate reservoir with strong water-drive. In: SPE/IATMI asia pacific oil & gas conference and exhibition. OnePetro; 2020.
[36] Sun CY, Liu H, Yan KL, Ma QL, Liu B, Chen GJ, et al. Experiments and modeling of volumetric properties and phase behavior for condensate gas under ultra-high-pressure conditions. Ind Eng Chem Res 2012;51:6916–25.
[37] Huang C. Characteristics of the condensate gas reservoirs in the north part of Talimu Basin and a discussion on their formation mechanism. Nat Gas Ind 1999;19:28–33.
[38] Wang SM, Lu XX. Features and petroleum significance of Ordovician carbonate reservoir in Tazhong area, Talimu Basin. J Xi'an Shiyou University (Natural Science Edition) 2004;19:72–6.
[39] Li GZ, Huang JQ, Ding Y. Evaluation of reservoir forming conditions of Dalaoba-II structure in Talimu Basin. J Xi'an Petrol Inst 2001;16:5–9.
[40] Tewari RD, Dandekar AY, Ortiz JM. Petroleum fluid phase behavior: characterization, processes, and applications. CRC Press; 2018.
[41] Keyvani F, Amani MJ, Kalantariasl A, Vahdani H. Assessment of empirical pressure–volume–temperature correlations in gas condensate reservoir fluids: case studies. Nat Resour Res 2019;29:1857–74.
[42] Zhang NL, Luo ZF, Chen ZX, Liu FS, Liu PL, Chen WY, et al. Thermal–hydraulic–mechanical–chemical coupled processes and their numerical simulation: a comprehensive review. Acta Geotechnica 2023:1–22.
[43] Coello CC, Lechuga MS. MOPSO: a proposal for multiple objective particle swarm optimization. In: Proceedings of the 2002 congress on evolutionary computation CEC'02 (cat No 02TH8600). IEEE; 2002.
[44] Wang CW, Peng XL, Liu JY, Jiang R, Li XP, Liu YS, et al. A novel formulation representation of the equilibrium constant for water gas shift reaction. Int J Hydrogen Energy 2022;47:27821–38.
[45] Wang CW, Wang J, Liu YS, Li J, Peng XL, Jia CS, et al. Prediction of the ideal-gas thermodynamic properties for water. J Mol Liq 2021;321:114912.
[46] Peng DY, Robinson DB. A new two-constant equation of state. Ind Eng Chem Fundam 1976;15:59–64.
[47] Lee ST, Jacoby RH, Chen WH, Culham WE. Experimental and theoretical studies on the fluid properties required for simulation of thermal processes. Soc Petrol Eng J 1981;21:535–50.
[48] Yuan GJ, Wan JF, Li JC, Li GT, Xia Y, Ban FS, et al. Stability analysis of a typical two-well-horizontal saddle-shaped salt cavern. J Energy Storage 2021;40:102763.
[49] Zhang J, Fang FF, Lin W, Gao SS, Li YL, Li Q, et al. Research on injection-production capability and seepage characteristics of multi-cycle operation of underground gas storage in gas field—case study of the Wen 23 gas storage. Energies 2020;13:3829.
[50] Zheng DW, Xu HC, Wang JM, Sun JC, Zhao K, Li C, et al. Key evaluation techniques in the process of gas reservoir being converted into underground gas storage. Petrol Explor Dev 2017;44:840–9.